CHAPTER 3
Mechanical & Fracture Behavior of Plasser & RDSO Wear Plate Samples & their Comparative Analysis

CHAPTER 3

Mechanical & Fracture Behavior of Plasser & RDSO Wear Plate Samples & their Comparative Analysis

3.1 Introduction

Ballast cleaning machines are essential equipment used in the maintenance and repair of railway tracks. A wear plate is a robust, durable component that is installed in ballast cleaning machines (BCM) to withstand the abrasive forces and wear caused by constant contact with ballast stones and debris. It serves as a protective layer that shields the underlying structure of the machine from damage, ensuring efficient operation and longevity. This study helps in evaluating the mechanical and fracture behavior of two distinct wear plates used in ballast cleaning machines. The tensile test & fracture test was conducted on universal testing machine (100KN capacity) for evaluating the percentage elongation vs strength criterion for both the samples in which Plasser sample has UTS about 1270 MPa and % Elongation about 18% and RDSO sample has UTS about 1195 MPa and %Elongation about 21%. Fatigue crack growth rate (FCGR) test is conducted to evaluate the behavior of both RDSO and PLASSER sample to monitor the crack growth rate& fracture toughness of both the samples through compact tension(CT) test was done followed by fractography of CT samples were studied through FESEM which shows the kind of fracture morphology. A brittle mode of fracture was observed in the Plasser-samples whereas a comparatively fibrous failure was observed in the RDSO-samples due to the presence of inclusions. In contrast PLASSER sample showcase good properties due to higher proportion of high-angle grain boundaries, a high dislocation density, smaller grain size.

The foundational material beneath the track that gives rails and sleepers stability and support is called ballasts. Ballasts, which are often made of gravel or crushed stone, are essential for maintaining track alignments, dispersing weights, and providing stability. However, the buildup of impurities like dust, dirt, and worn material from rail activity causes this essential ballast bed to deteriorate over time. Machines for cleaning ballast are essential to restoring the train network. fig.3.1 describes the ballast cleaning machine and wear plates used in it.

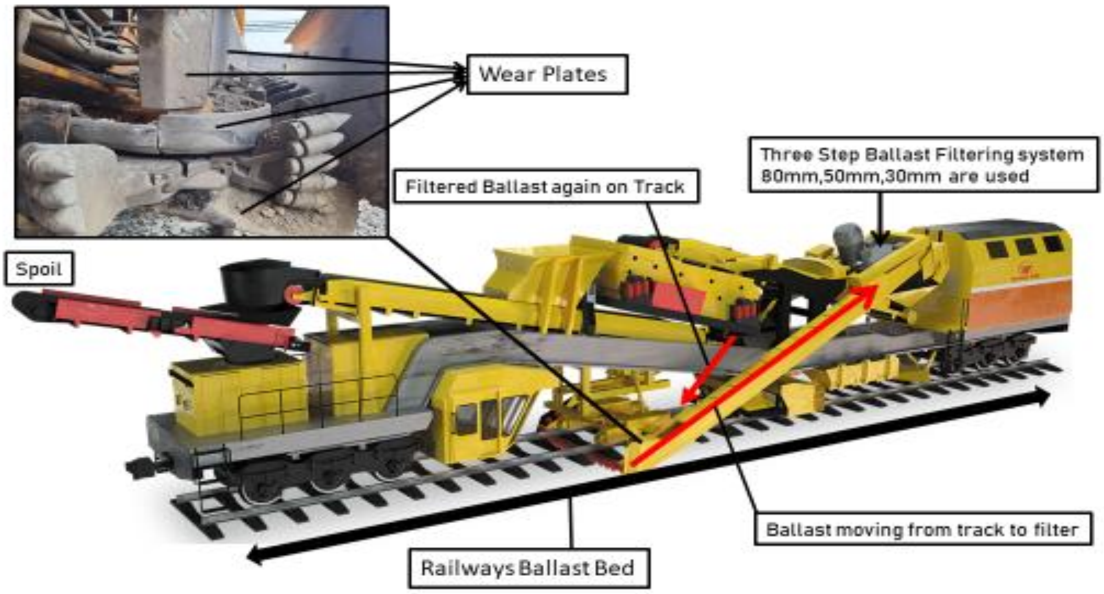

Fig.3.1: Typical view of ballast cleaning machine and wear plate

In order to provide the best track geometry and stability, these specialist machines are designed to remove and recycle the worn-out ballast while also adding new material to it. Increasing the service life of train tracks by using efficient and economical railway maintenance techniques [71]. Because of their remarkable mechanical qualities and resistance to wear and abrasion, alloy steels are widely applicable as wear plates in heavy machinery. BCM (Ballast cleaning machines) are essential for preserving the stability and integrity of railroad lines because they remove debris and contaminated ballast [72].

In connection with the track arrangement, the ballast is cleaned in an 800 m long section with an excavation depth of 350 mm. On average, 60% of the ballast can be recycled. This enables huge savings regarding both this expensive resource and its transport. Cleaned and new aggregate is returned to the track layer by layer. A dynamic track stabilizer homogenizes each layer [73]. This makes it possible to increase the lateral movement resistance of the railway network. Along with the targeted starting count of the track, the maintenance intervals are extended. The next work steps are the delivery of new ballast, two compact runs, dynamic track stabilization and overhead line adjustment [74]. The track can receive a maximum speed of 300 km/h after loosening the track and final lifting and coating. To do this, the rails are cut to a certain length to eliminate the stresses that arise during maintenance. The rails are then joined back together to form a continuously welded track. For the wear plates of the ballast cleaning machine generally we used the steel grade 31Ni10Cr3Mo6 (IS: 5517-1993) in tempered and hardened condition.

The performance and service life of wear plates determine how well the ballast cleaning process works. Important machine parts are shielded from wear by the wear plates, which are frequently made of tempered and hardened high-strength alloy steels with exceptional tensile strength and fracture toughness qualities [75].

The current study examines the overall effects of alloying elements and microstructural parameters on the performance of wear plates used in blast cleaning operations through a comparative examination of fracture toughness & tensile strength performance [76]. The following highlights the novelty of the current investigation on the tensile strength and fracture toughness of samples S1 (Plasser) and S2 (RDSO) for wear plates used in ballast cleaning machines:

- The present research delves into the Yield strength (YS), Ultimate tensile strength (UTS) and Percentage elongation (%El) of samples Plasser S1 and RDSO S2 which shows the variation due to different compositions.
- The present study delves into the variation in the fracture toughness of samples S1 and S2.
- The factographs shows the behavior and nature of fractured surface of both the samples S1 and S2 during fracture toughness testing.

3.2 Materials & Method:

Sample S1 served as a wear plate within the Plasser & Theurer (FRM80) ballast cleaning machine and was crafted from high-grade German steel. Sample S2 provided by RDSO comprised Steel Grade 31Ni10Cr3Mo6, adhering to the IS: 5517-1993 specification for Hardening and Tempering Steel.

Table 3.1: Composition analysis obtained by XRF (X-ray fluorescence) analyzer [77] for the sample S1, and S2.

Wear plate sample	Constituent Elements (wt.%)							
	C	Si	Mn	Cr	Ti	Mo	Co/Cu/Nb/Ni	Fe (Balance)
S1 Plasser	0.1095	0.379	1.484	0.240	0.0265	0.118	<0.02	>97.5
S2 RDSO	0.0323	0.354	1.351	0.369	0.085	0.081	<0.02	>97.5

Table 3.1 shows the composition of as-received wear samples S1, and S2 obtained using XRF (X-ray fluorescence) analyser. Non-destructive XRF (X-ray fluorescence) can be used to determine a material's elemental composition [78].In XRF analysers, the chemical composition of a sample is determined by measuring the fluorescent (or secondary) X-rays released from the sample upon excitation by a primary X-ray source.The XRF spectroscopy method is an excellent way to analyze the composition of materials qualitatively and quantitatively [79]. It is evident from the analysis that the sample S1 has a relatively higher amount of C, Si, Mn and Mo as compared to sample S2.

3.3 Material characterization

Flat specimens of the "dog bone" type for tensile test and CT specimen for fatigue crack growth Rate &fracture test were cut and had a 30 mm gauge length and 3*7 mm^2 cross section and Using the ASTM-E561 standard, standard compact tension (CT) specimens were introduced [80]. To prepare the specimens and create pre-cracks in them, a wire cutting machine was used. The specimens have dimensions of 34 mm × 34 mm × 3 mm. Furthermore, a 60° V-notch was made [81]. The notch was machined at an equal distance from the top and bottom margins of the specimen, and perpendicular to the loading axis as illustrated in figure 3.2.

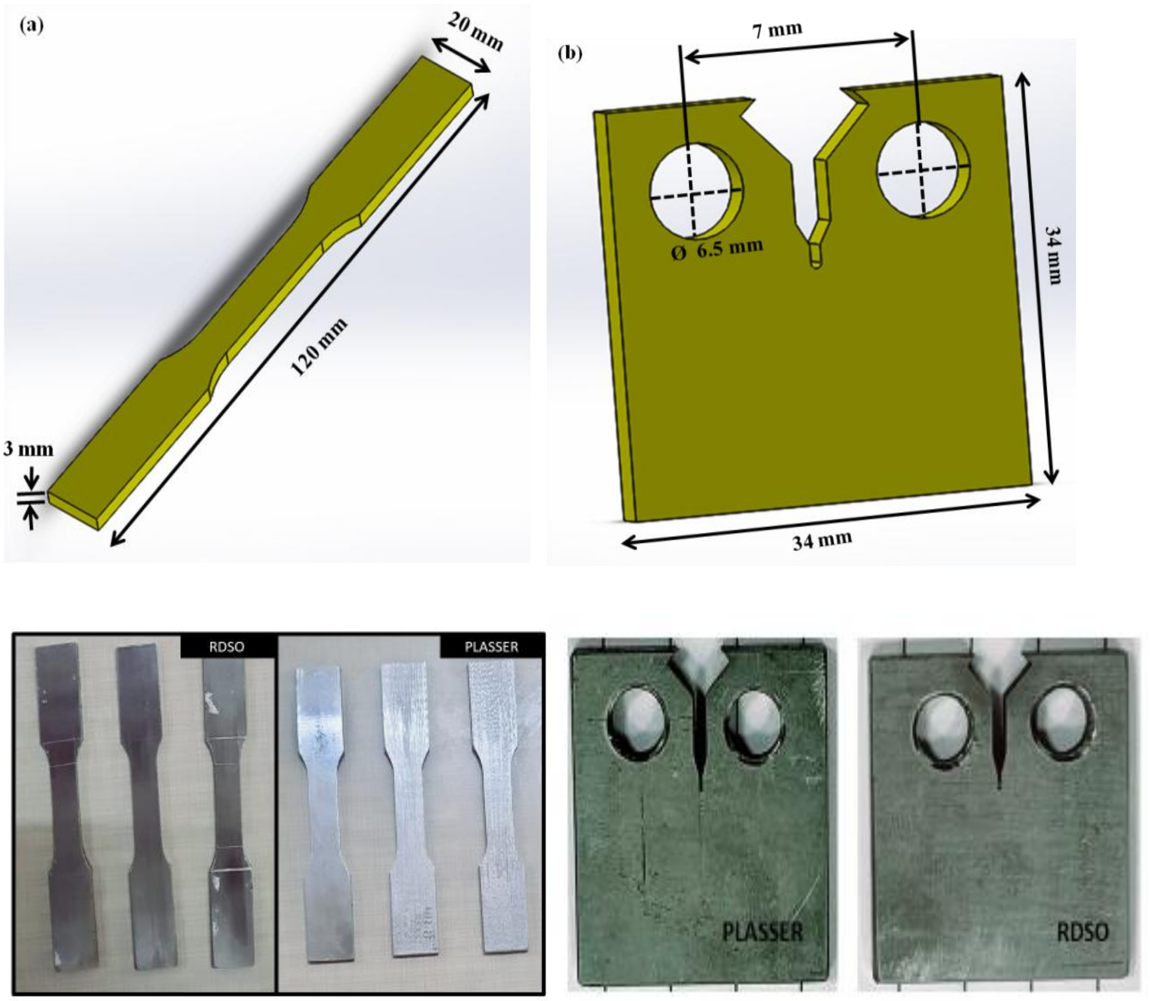

(c) (d)

Fig 3.2: Dimension of various specimen (a) Tensile Specimen 3D Model (b) CT Specimen 3D Model (c) Actual Tensile Specimen Plasser & RDSO (d) Actual CT Sample of Plasser & RDSO

Instron testing devices were used to perform uniaxial tensile tests J1C at room temperature with a strain rate of $1*10^{-3}$ s^{-1}. Mechanical characteristics were averaged over two samples at each experimental point [82]. figure 3.3 shows the Instron 100KN Machine, which is used to conduct both tests.

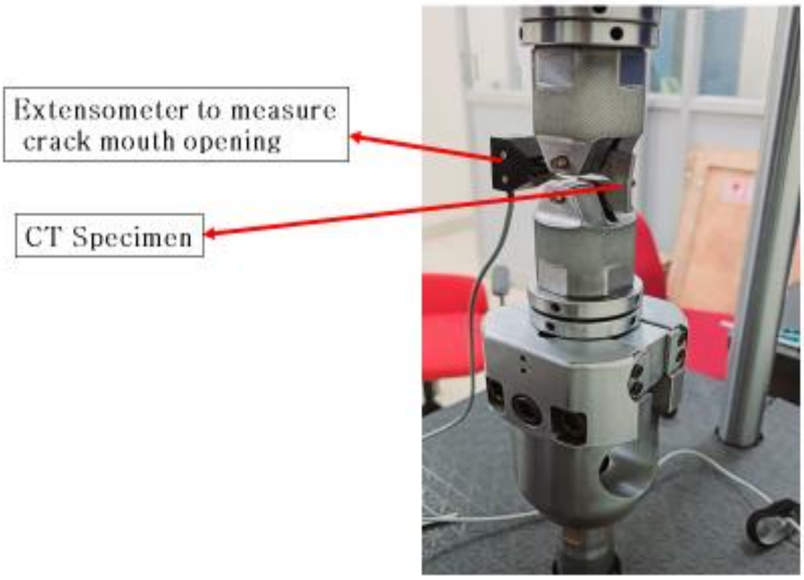

Fig 3.3: Schematic view of Instron100KN Testing Machine & CT Specimen

Local geometry and defects cause plastic deformation at the crack tip at low stresses, resulting in fatigue crack growth [83]. The crack tip becomes sharper during the loading and unloading cycle, increasing the stress concentrator locally. This happens cyclically, which leads to the crack growing Δa. The stress field at the crack tip & the stress intensity factor, K, and are connected. Since the highest applied stress during the cycle is distant from the material's yield strength, there will be small scale yielding at the crack tip and the application of linear elastic fracture mechanics is feasible. As a result, a crack's growth, Δa, can be connected to ΔK. For the structure or specimen to fail completely, a high number of cycles are required, typically more than 10,000 and the failure mechanism is referred to as high cycle fatigue.

Experiments show that fatigue cracks grow by Δa for each cycle, with the size of the Δa increasing with increasing load amplitude [84]. Therefore, the growth of fatigue cracks can be expressed as function of ΔK:

$$\frac{da}{dN} = F(\Delta K)$$

The overall behavior of fatigue fracture formation in metallic materials can be characterized by the curve in figure 3.4 that shows the fluctuation of da/dN against ΔK. In actuality, FCG depends on a number of other variables as well, including the environment, waveform, frequency, and stress ratio [85-89]. There are three distinct regimes represented by this sigmoidal curve, each exhibiting unique behavior.

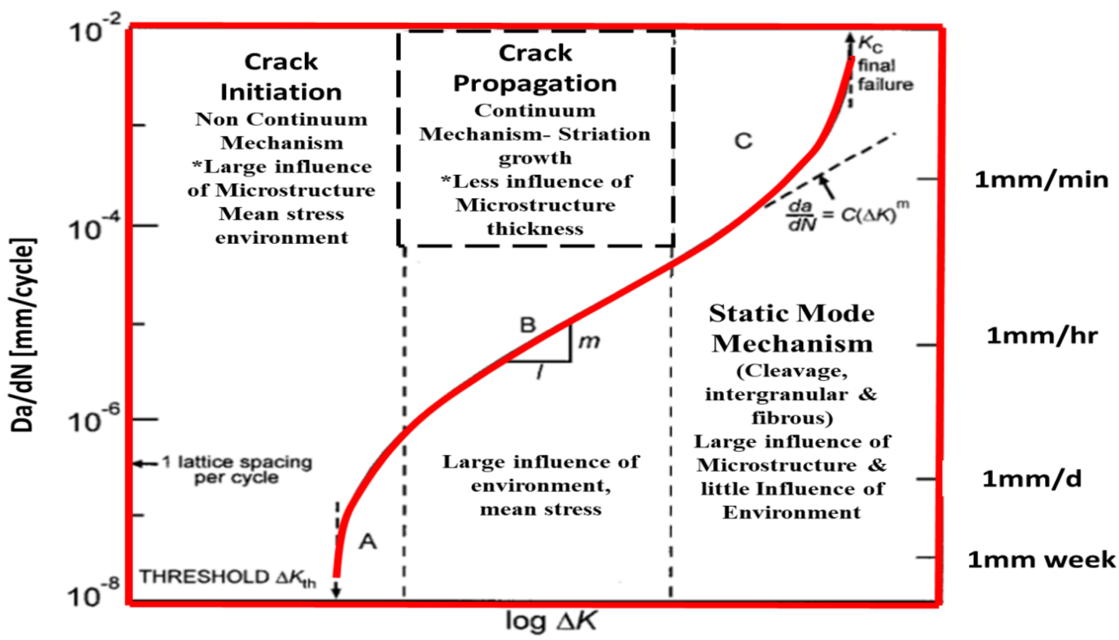

Fig.3.4: da/dN vs ΔK curve showing crack growth rate at 50Hz

In regime-A, In this regime, the crack propagates along the crystalline planes of the material, the high-shear stress planes at 45 degrees. Because the plastic zone is enclosed inside the grains of the material, it spreads until it is slowed down by inclusions, grain boundaries, or other microstructure obstacles. That's why stress level and microstructure have a big impact on FCG in this regime [90]. This is where the threshold is specified. When ΔK is equal to or less than ΔK_{th}, it is assumed that the propagation has halted or is happening at non-detectable rates. This is because FCG is very slow in this scenario [91-95].

In regime B, The Paris Law describes the linear dependency between log (da/dN) vs log(ΔK) at this stage as follows:

$$\frac{da}{dN} = c(\Delta k)^{\mathrm{m}}$$

In this case, c and m are empirically obtained material properties. The constant m, whose value typically ranges from 2 to 5, denotes the crack tip's sensitivity to the load [96].

The last failure, which might be ductile or fragile depending on the material's mechanical characteristics, happens in regime C [97].

3.4 Tensile properties

Tensile tests on two different steel samples with varying carbon compositions to investigate their mechanical propertiesS1 demonstrated significantly higher tensile strength and yield strength but with reduced ductility.

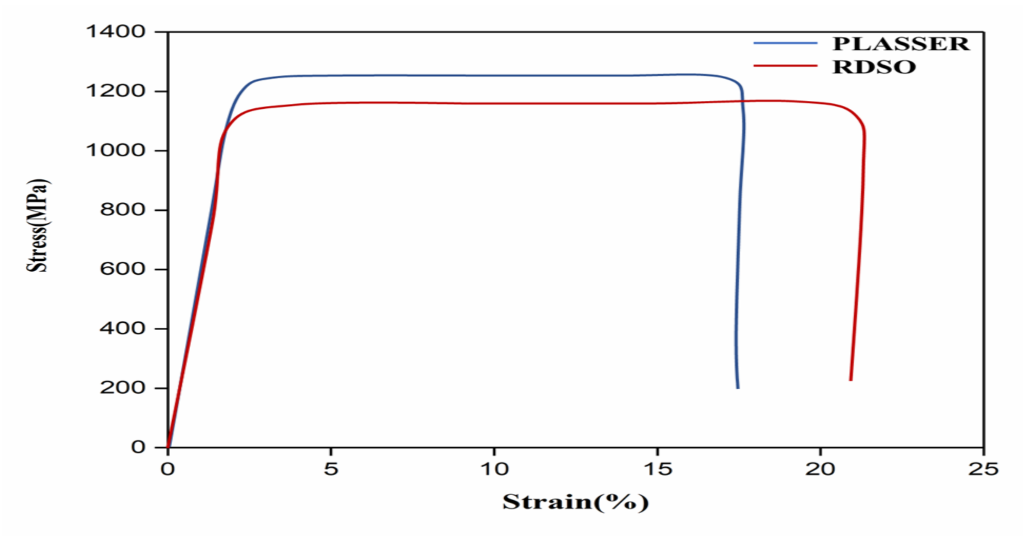

Figure 3.5: Typical engineering stress strain curve

Figure 3.5 shows the variations of stress and strain for different samples we found that sample S1 has large UTS about 1270 MPa and 18% percentage elongation whereas S2 has UTS about 1190 MPa and 21% percentage elongation. The reason behind this variation is percentage of carbon and also variation in grain size [98-99].

3.5 FCGR (Fatigue crack growth rate)

Fatigue crack growth rate (FCGR) test is conducted to evaluate the behavior of both RDSO and PLASSER sample. The FCGR test involves cyclic loading of a pre-cracked specimen at varying stress intensity levels (delta K), while monitoring the rate of crack growth (da/dN). The da/dN vs delta K curve obtained from the test provides crucial insights into the material's fatigue resistance and crack propagation characteristics [100]. This curve is essential for determining the alloy's fatigue crack growth behavior, critical crack sizes, and estimating its remaining fatigue life under specific loading conditions.

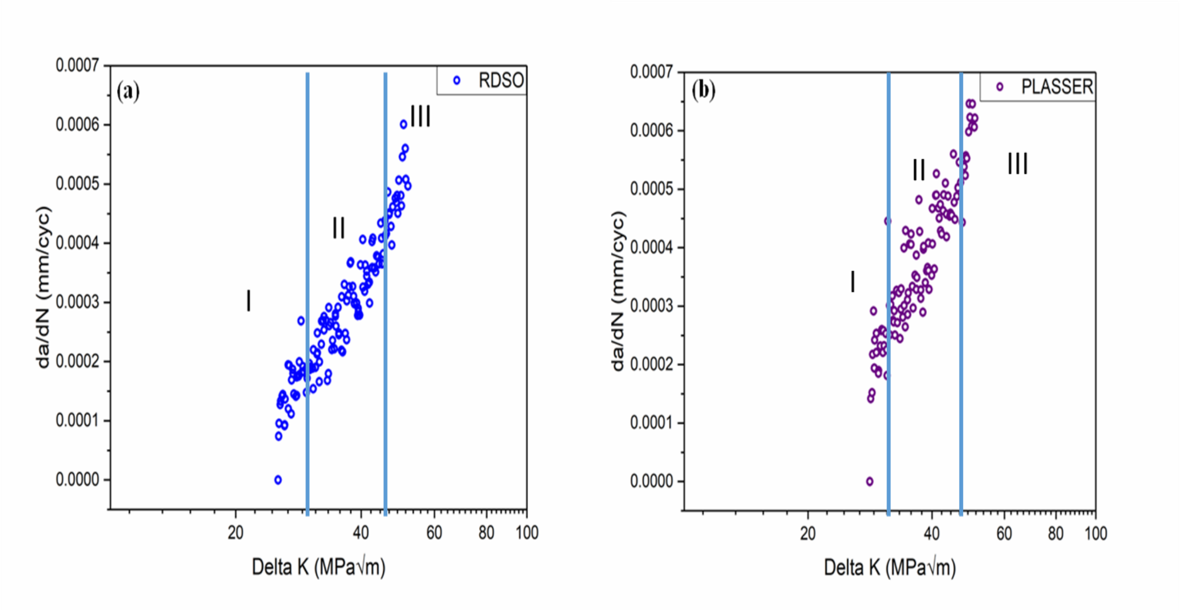

Figure 3.6-Typical FCGR curve (a) RDSO (b) PLASSER

The RDSO and PLASSER samples' tested FCGR results are shown in the above figure 3.6. The data primarily represents growth rates in the intermediate crack growth regime, between -5*10-5 mm/cycle and 7*10-4 mm/cycle, it could be seen for R-ratio 0.3

fatigue growth rate is approximately linear this linearity is favorable further more it can be seen that PLASSER sample is more resistive to fatigue fracture because of influence of microstructure.

3.6 J1C Test (Plane stress fracture toughness)

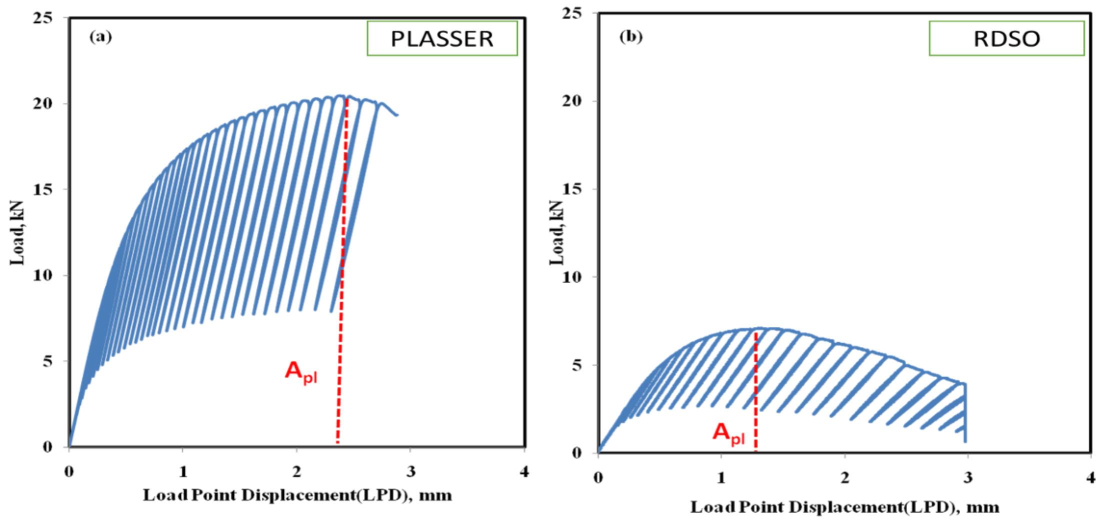

(a) (b)

Figure 3.7-Typical LDP curve (a) PLASSER (b)RDSO

To take into consideration the materials' elastic-plastic behavior, the J-Integral was assessed. For the plane stress fracture toughness (JI) test, a small thickness specimen with a large size of plastic zone around the crack tip is needed. Begley and Landes created an experimental technique based on J-Integral [101]. They employed CT specimens with varying beginning crack lengths, and each specimen's load-displacement relationship was measured using a tensile test apparatus. fig 3.7 shows better performance and fracture toughness of S1 sample. Another approach of calculating fracture toughness is numerical method [102].

3.7 Load point displacement Curve

The following equation provides the plane stress fracture toughness, which was determined using the LPD-load curve theory (ASTM E1820-13)

$$j = \frac{(1-\mu^2)K^2}{E} + J_{pl} \qquad (1)$$

$$J_{pl} = \frac{\eta_{pl} A_{pl}}{bB_N} \qquad (2)$$

As from the above curve A_{pl} is the maximum area from the origin upto peak load as shown in figure and also b is the unbroken ligament [103].

$$b = W - a \qquad (3)$$

$$\eta_{pl} = 2 + 0.522\frac{b}{w} \qquad (4)$$

In case of Fe alloys ; E=210 GPa and μ=0.25 We get

The plane stress fracture toughness for S1 is $98kJ/m^2$ and for S2 is $83kJ/m^2$.

3.8 Fractography

Fractography images for the two samples are shown in the figure below. The first noticeable difference between the two images (Fig 3.8 a, b) is the absence of inclusion particles in the S1 (Plasser) (fig 3.8a) sample. Irregular arrangement between metal and inclusion interface leads to stress concentration which may lead to crack initiation from the interface and ultimately extends resulting in material failure [104]. This explains the fact that Plasser sample S1 has a higher UTS as compared to its counterpart. Also, the mode of fracture in the S1 sample is more of a brittle one as the fracture surface has facets leading to cleavage which is typical in a brittle material (fig 3.8c). Cleavage fracture usually occurs along crystallographic planes. A key feature in this type of fracture is the presence of flat facets, typically about the size of a ferrite grain (in steel). These flat facets mostly display "river markings" (fig. 3.8 a). These river markings result from the crack traveling through the crystal along several parallel planes, making a series of plateaus and connecting ledges indicating energy absorption through local deformation [105]. The direction of the "river pattern" refers to the direction of crack propagation. The fracture surface of the S2 sample is comparatively more fibrous leading to a dimpled rupture (fig. 3.8 b, d) which explains the higher ductility observed in the sample.

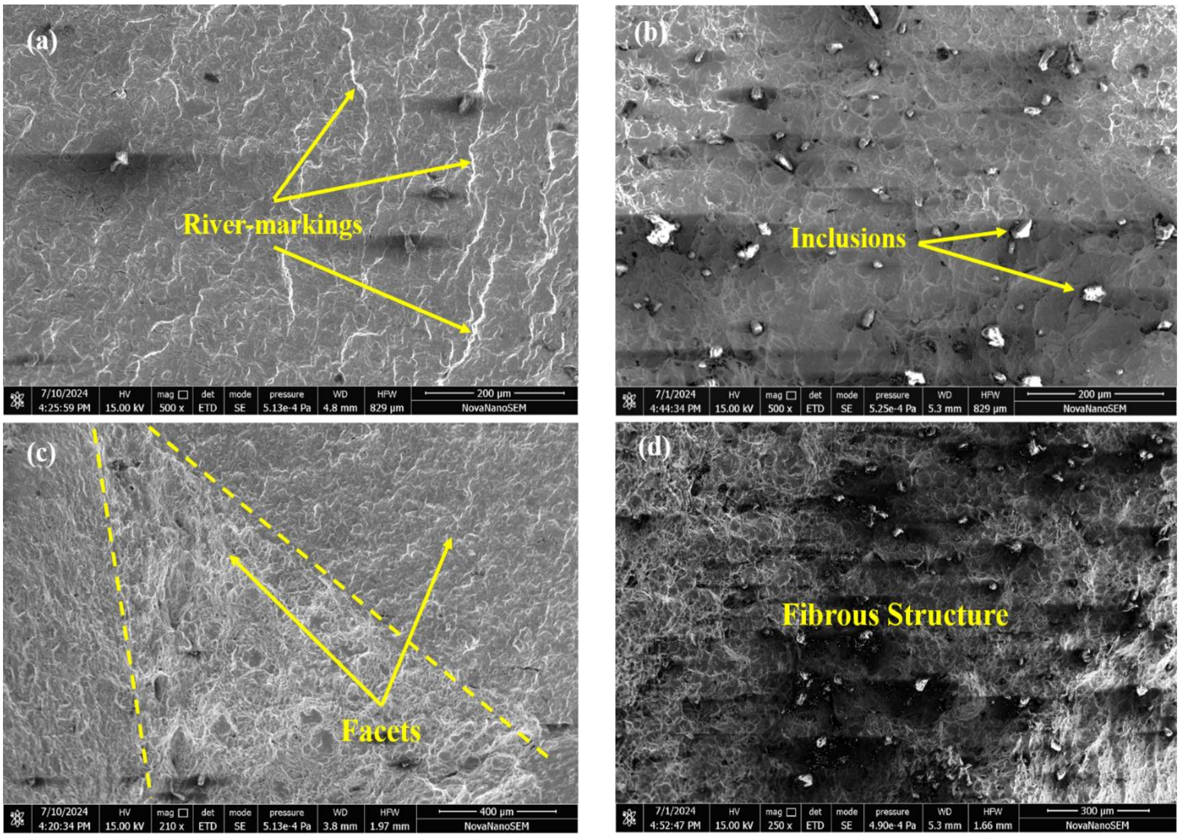

Fig 3.8: Fractography images of (a) S1-sample at 500X and (b) S2-sample at 500X (c) S1-sample at 200X (d) S2-sample at 250X

3.9. Discussion

3.9.1 Effect of alloying element on mechanical properties-

The strength and ductility of steels are also profoundly influenced by carbon content. S1, with a higher carbon concentration, demonstrated enhanced strength but reduced ductility compared to S2, which contained a lower carbon percentage. As we know that carbon is a interstitial solute so it occupies the interstitial sites and enhance the strength on expanse of ductility. Further Carbon, when alloyed with iron in steel, primarily occupies interstitial sites within the iron crystal lattice [106]. This means that carbon atoms fit into spaces between the iron atoms rather than replacing iron atoms in the lattice structure. This interstitial occupancy is a key factor that profoundly influences the mechanical properties of steel [107]. The presence of carbon atoms in these interstitial sites disrupts the regular crystal structure of iron, known as ferrite, and creates a solid solution known as austenite when the steel is heated to high temperatures. Upon cooling, depending on the carbon content and the cooling rate, the steel can transform into different microstructures such as pearlite, martensite, or bainite, each with distinct mechanical properties [108]. Higher carbon content generally results in increased strength due to the formation of harder and stronger phases like martensite during quenching [109]. However, higher carbon content can also lead to reduced ductility and toughness, as it tends to make the steel more brittle and prone to fracture.

The wear plate sample S1 was found to have higher content of alloying elements like C, Si, Mn & Mo. In Plasser sample higher silicon percentage increases the amount of retained austenite and its mechanical and thermal stability, which can lead to improvements in the steels' strength and toughness [110]. The higher amount of manganese in Plasser sample as compare to RDSO sample increases its hardenability by lowering the critical cooling rate during the hardening process. In plasser sample molybdenum percentage is higher than in RDSO sample, it strengthens ferrite in solid solutions and increases carbide stability. The ductility, toughness, and wear resistance of steel are all improved by it. Molybdenum significantly boosts ferrite's creep resistance and raises the softening and re crystallization temperatures following deformation strengthening.

3.9.2 Fractography:

This microstructure's high density of high-angle boundaries, which usually serve as barriers to cleavage propagation, is associated with its strong toughness (reported in the previous study). The cleavage crack is compelled by these constraints to modify its microscopic propagation plane in order to conform to the local crystallography. Low-angle boundaries, on the other hand, do not significantly affect the toughness of steel since they are not effective in preventing cleavage. Lath-like upper bainite, however, demonstrates a strong balance of strength and toughness due to its high internal dislocation density and fine grain structure [111].

In high-magnification micrographs, the fracture initiation site can be identified by tracing river lines; nevertheless, the initiation site itself frequently lacks features. Although research into the locations where cracks and/or voids initiate in these microstructures is still in progress, hard grains are thought to be the most vulnerable to the formation of micro-voids and microcracks [112]. The fractographs in Fig. 8 show that sample S1 with granular bainite morphology have transgranular facets on the cleavage fracture surface compared to sample S2. Accordingly, the rapid diffusion of microcracks across bainitic ferrite boundaries is the main mechanism governing the brittle fracture of cementite-free bainitic steels chilled continuously [113]. Because they do not blunt fracture formation like ferrite does, hard, brittle phases perform an important intermediary role.

3.10 Conclusion

This study focused on the fracture behaviour of samples S1 (Plasser) and S2 (RDSO), with particular attention to their microstructural features and toughness. It was concluded that the brittle fracture in the S1 sample can be attributed to a microstructure characterized by transgranular facets on the cleavage fracture surface, while the more fibrous failure in the S2 sample is associated with the presence of inclusions that contributed to crack arresting. The microstructural analysis indicates that high-angle grain boundaries played a significant role in the toughness observed in both samples, as these boundaries forced the cleavage cracks to alter their propagation path, enhancing fracture resistance.

The following key findings were produced in this study:

- Sample S1 exhibits a large UTS of approximately 1270 MPa and 18% percentage elongation, while sample S2 displays a UTS of approximately 1190 MPa and 21% percentage elongation which shows that sample S1 have better performance.
- The FCGR test indicates that the PLASSER sample exhibits greater resistance to fatigue fracture due to the impact of its microstructure.
- Tensile test indicates higher yield strength with a lower toughness and ductility for the Plasser samples as compared to the RDSO samples.
- The granular bainitic morphology of sample S1 showed transgranular cleavage facets, which promoted microcrack formation and rapid propagation across bainitic ferrite boundaries.
- Hard grains within the microstructure were identified as potential nucleation sites for micro-voids and microcracks, contributing to the brittle nature of sample S1.
- A brittle mode of fracture was observed in the Plasser-samples whereas a comparatively fibrous failure was observed in the RDSO-samples due to the presence of inclusions.

- The plane stress fracture toughness for S1 is $98 kJ/m^2$ and for S2 is $83 kJ/m^2$ which means Plasser sample is better than localized RDSO sample.